5-5-2005

Stretching and mixing of non-Newtonian fluids in time-periodic flows

Paulo E. Arratia
University of Pennsylvania, parratia@seas.upenn.edu

Greg A. Voth
Wesleyan University

J. P. Gollub
Haverford College

Suggested Citation:
Arratia, Paulo E., Greg A. Voth, J.P. Gollub. (2005). *Stretching and Mixing of Non-Newtonian Fluids in Time-Periodic Flows.* Physics of Fluids. Vol. 17. Art. 053102.

NOTE: At the time of publication, author P.E. Arratia was affiliated with Haverford College. Currently (as of July 2007), he is a faculty member in the Department of Mechanical Engineering and Applied Mechanics at the University of Pennsylvania.

Stretching and mixing of non-Newtonian fluids in time-periodic flows

Abstract
The stretching of fluid elements and the dynamics of mixing are studied for a variety of polymer solutions in nearly two-dimensional magnetically driven flows, in order to distinguish between the effects of viscoelasticity and shear thinning. Viscoelasticity alone is found to suppress stretching and mixing mildly, in agreement with some previous experiments on time-periodic flows. On the other hand, the presence of shear thinning viscosity (especially when coupled with elasticity) produces a dramatic enhancement in stretching and mixing compared to a Newtonian solution at the same Reynolds number. In order to understand this observation, we study the velocity field separately in the sheared and elongational regions of the flow for various polymer solutions. We demonstrate that the enhancement is accompanied by a breaking of time-reversal symmetry of the particle trajectories, on the average. Finally, we discuss possible causes for the time lags leading to this temporal symmetry breaking, and the resulting enhanced mixing.

Disciplines
Engineering | Mechanical Engineering

Comments
Suggested Citation:
Arratia, Paulo E., Greg A. Voth, J.P. Gollub. (2005). *Stretching and Mixing of Non-Newtonian Fluids in Time-Periodic Flows.* Physics of Fluids. Vol. 17. Art. 053102.

NOTE: At the time of publication, author P.E. Arratia was affiliated with Haverford College. Currently (as of July 2007), he is a faculty member in the Department of Mechanical Engineering and Applied Mechanics at the University of Pennsylvania.

Stretching and mixing of non-Newtonian fluids in time-periodic flows

P. E. Arratia
Department of Physics, Haverford College, Haverford, Pennsylvania 19041

Greg A. Voth
Department of Physics, Wesleyan University, Middletown, Connecticut 06459

J. P. Gollub
Department of Physics, Haverford College, Haverford, Pennsylvania 19041 and Department of Physics, University of Pennsylvania, Philadelphia, Pennsylvania 19104

(Received 13 July 2004; accepted 21 March 2005; published online 5 May 2005)

The stretching of fluid elements and the dynamics of mixing are studied for a variety of polymer solutions in nearly two-dimensional magnetically driven flows, in order to distinguish between the effects of viscoelasticity and shear thinning. Viscoelasticity alone is found to suppress stretching and mixing mildly, in agreement with some previous experiments on time-periodic flows. On the other hand, the presence of shear thinning viscosity (especially when coupled with elasticity) produces a dramatic enhancement in stretching and mixing compared to a Newtonian solution at the same Reynolds number. In order to understand this observation, we study the velocity field separately in the sheared and elongational regions of the flow for various polymer solutions. We demonstrate that the enhancement is accompanied by a breaking of time-reversal symmetry of the particle trajectories, on the average. Finally, we discuss possible causes for the time lags leading to this temporal symmetry breaking, and the resulting enhanced mixing. © *2005 American Institute of Physics*. [DOI: 10.1063/1.1909184]

I. INTRODUCTION

Twenty years ago, Aref[1] demonstrated that simple, time-periodic flows in two dimensions can produce mixing and complex distribution of materials by chaotic advection. The majority of previous research on mixing in time-periodic flows, with exceptions to be discussed below, has been restricted to Newtonian fluids.[2–7] Most practical viscous fluids, in contrast, contain polymers or particles (e.g., polymer melts, pastes, and colloids) and are not Newtonian. Examples occur in cell fermentation, polymer processing, volcanic flows, and synovial fluid flow in joints. An important feature of many non-Newtonian fluids is that they often exhibit both viscoelasticity and shear-thinning viscosity, particularly solutions containing flexible polymers.

Flow instabilities, irregular flow patterns, and nonlinear dynamics have long been observed in purely elastic fluids[8–13] and in fluids possessing both elasticity and shear-thinning viscosity.[14–16] Most of the nonlinear flow behavior observed in these studies arises from the extra elastic stresses due to the presence of polymer molecules. Mechanical stresses in these fluids are history dependent and depend on a characteristic time λ that in dilute solutions is proportional to the relaxation time of a single polymer molecule. In semidilute solutions, λ depends also on molecular interactions. These stresses grow nonlinearly with strain rate and can dramatically change the flow behavior. A common example is the rod-climbing or Weissenberg effect in curvilinear flows, where a viscoelastic fluid creeps up a rod being rotated in the medium. The fact that viscoelastic fluids can lead to flow bifurcations is of interest in fluid mixing. Despite advances in understanding fluid mixing and recognition of the importance of non-Newtonian fluids, few studies have focused on the mixing of such fluids.

The majority of the non-Newtonian mixing studies have focused either solely on viscoelasticity[17–21] or on shear-thinning viscosity,[22] but few have focused on the interaction between these two phenomena. Viscoelasticity is most often investigated using constant-viscosity, elastic fluids,[23] which minimizes shear-thinning effects. In previous experiments on time-periodic flows of such fluids, mixing has been found to be retarded in some cases,[17] and enhanced in others.[18] A dramatic example of mixing enhancement has been seen for experiments in small curved channels.[24] On the other hand, shear-thinning viscosity has been shown computationally to have a potentially large impact on fluid mixing by decreasing the degree of Lagrangian chaos in time-periodic flows.[22] Nevertheless, non-Newtonian fluids often exhibit both shear-thinning and viscoelastic behavior and it is difficult to know *a priori* the effects of their interaction on mixing by studying them separately. There are a few early mixing investigations dealing with shear-thinning-viscoelastic fluids, but they focus mainly on macroscopic measures such as torque requirement and power consumption.[25,26] More recently, an experimental study in a torsionally driven cavity[27] found certain differences in flow behavior between Boger and slightly shear-thinning fluids, but no general conclusions on the effect of shear thinning on mixing are drawn.

In this paper, we investigate the effects of both viscoelasticity and shear-thinning viscosity individually and together on fluid mixing. We study the velocity fields quantitatively using particle tracking with unusually high precision and resolution. By doing so, we can also study the stretching

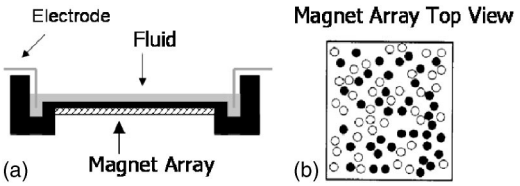

FIG. 1. Schematic diagrams of (a) the two-dimensional, magnetically forced, time-periodic flow, and (b) the random arrangement of forcing magnets. Dark and white circles indicate magnet polarity.

of fluid elements, a critical determinant of mixing. While previous methods allow the stretching of isolated fluid elements to be determined, our approach[28] allows the *stretching fields* to be determined. These two-dimensional fields quantitatively characterize the stretching process at each location, both in the future and in the past of a given instant, everywhere in a two-dimensional flow. Stretching is intimately related to the rate of divergence of initially nearby points, which in chaotic flows is exponential in time on the average, and can be used as a measure of mixing efficiency.[2] For time periodic flows, stretching fields label the stable and unstable manifolds of fixed points of flow maps, and can be used to characterize the mixing dynamics or in some cases to predict mixing rates.[29] Hence, the statistical and geometric properties of the experimentally calculated stretching fields are powerful tools for characterizing mixing in fluids.

This paper is organized as follow. We describe in Sec. II the experimental setup and rheology of the fluids investigated here. The role of elasticity on fluid mixing is investigated in Sec. III by first comparing the mixing of a Boger fluid to a viscosity-matched Newtonian fluid and then by investigating the effects of shear-thinning viscosity using fluids with different levels of elasticity. A novel type of flow analysis is also presented in Sec. III, where we study the flow profiles separately in sheared and elongational regions of the flow. Our summary and conclusions follow in Sec. IV. We find that the presence of shear-thinning viscosity substantially modifies the velocity fields and produces a large enhancement of stretching and mixing. The effect is largest if viscoelasticity is also present. On the other hand, a small level of elasticity alone (without shear thinning) reduces stretching and mixing somewhat compared to the Newtonian case under the same conditions (geometry and Reynolds number).

II. EXPERIMENTS

We investigate mixing in an electromagnetically driven thin fluid layer as shown in Fig. 1. A time-periodic current travels horizontally through a fluid layer that is placed above an array of permanent magnets. We use 92 magnets (1.2 cm in diameter) with a 2 cm mean spacing. The resulting Lorenz forces drive a time-periodic vortex array flow in the fluid. The magnets are placed and oriented randomly as shown in Fig. 1. The area of fluid flow is 15×15 cm^2, and all figures in this paper show a central 11×11 cm^2 region. The typical forcing frequency is 100 mHz and typical velocities are 0.07–1.2 cm/s. For all experiments, the fluid of interest is a 1 mm thick nonconductive layer that floats on top of a 3 mm denser conductive layer. Note that both fluid layers have the same composition, except that the lower layer is made conductive and denser by the addition of 5% by weight of KCl salt. The two layers remain distinct for the duration of the experiments, even though they are miscible. We use two layers to ensure the two dimensionality of the thin upper layer (see below).

For dye experiments, half of the upper layer is initially marked with fluorescein at a concentration of $(6\times10^{-5})M$ while the other half remains unmarked by dye. The diffusivity of fluorescein is $D=5\times10^{-10}$ m^2 s^{-1}. Particle tracking experiments are performed by seeding the system with fluorescent polystyrene spheres 120 μm in diameter. Tracer particles are placed at the interface separating the two fluid layers. Usually, 600–800 particles are imaged in a single frame. We record up to 8000 images using a charge-coupled device camera (512×512) at 8 Hz in a typical run, or 80–100 images per period. The centroid of each particle is found with a precision of 48 μm. Particles found in sequential images are then labeled and combined into tracks. The boundary conditions are the same for the dye and the particle tracking experiments; there is a free surface for both types of experiments.

Because the flow is periodic, we can combine particle positions obtained at a given phase (relative to the forcing) to obtain up to 80 000 precise particle positions at each phase and thereby obtain very high spatial resolution (0.004 of the field of view), excellent time resolution (0.01 of a flow period), and velocities accurate to a few percent.

The velocity fields are accurately two dimensional in the upper layer, because the period of the flow variation is quite long compared to the vertical momentum transport time across the upper layer (typically 10 s vs 0.2 s for the viscous solutions used here). Therefore, vertical gradients of the horizontal velocity are negligible. This issue has been discussed in previous work on Newtonian fluids in the same geometry,[29,30] but the two-dimensional approximation is even better here because of the high viscosity. We also find that the horizontal divergence $\partial u/\partial x+\partial v/\partial y$ of the velocity field, on average, differs from zero by less than 0.05% of the typical horizontal mean shear rate (defined in the "Fluid rheology" subsection, below).

The process of extracting stretching fields begins by using polynomial fitting to determine particle velocities, which are then interpolated onto a grid. Flow maps are constructed by integrating hypothetical particle trajectories numerically using the velocity grids. These maps determine the final destinations (after an interval $\Delta t=0.125$ s) of particles as a function of their initial positions. Finally, the stretching fields are determined from gradients of the flow maps. One can most easily comprehend these fields by regarding them as measuring the deformation of an initial small circle (at a given spatial location) into an ellipse; the ratio of the major diameter to the initial diameter is the stretching, but it is actually computed as the largest eigenvalue of the right Cauchy–Green strain tensor at the point in question.[28]

Two different quantities are computed at each point, which we call future and past stretching. Future stretching is the stretching experienced by a fluid element in the next Δt.

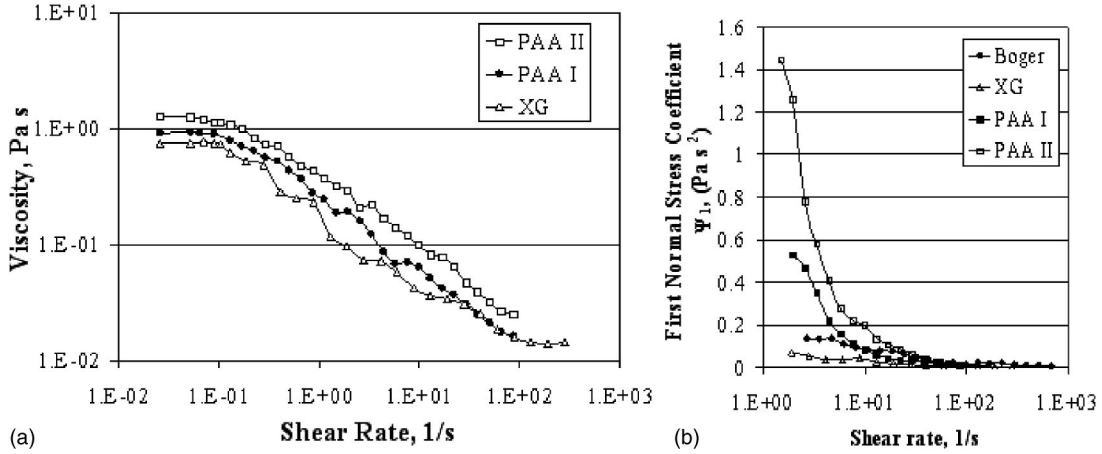

FIG. 2. (a) Viscosity curves and (b) first normal stress coefficient for the shear-thinning fluids used in this work. Lines connecting data points are added to guide the eye.

Past stretching is the stretching that a fluid element experienced in the previous Δt. The starting phase for future stretching measurements and the ending phase for past stretching measurements, corresponds to an instant at which the rms velocity is nearly constant, about 0.26 periods after the current is reversed. However, similar results are obtained at other phases. We estimate that the uncertainty in the mean stretching is about 4%. This uncertainty was estimated by adding random noise to the velocimetry data and computing stretching from the "noisy" velocimetry data. Further detail on the velocimetry measurements and stretching calculations may be found elsewhere.[28]

Fluid rheology

The polymers used are high-molecular-weight (MW) polyacrylamide (PAA, 18×10^6 MW, Polysciences) and xanthan gum (XG, 2.7×10^6 MW, Sigma-Aldrich). The former has a flexible backbone while the latter is a stiff "rodlike" polymer, with flow behavior that mimics suspensions of fibers in Newtonian media. The overlap concentrations C^* are 300 ppm and 170 ppm for the PAA and XG solutions, respectively. Despite its lower molecular weight, the xanthan gum solution has a lower overlap concentration than PAA, since it is a rigid polymer, having a higher effective volume fraction. These overlap concentrations correspond to molecular concentrations $n_{\mathrm{PAA}}=1.01\times10^{13}$ molecules/cm^3 and $n_{\mathrm{XG}}=3.79\times10^{13}$ molecules/cm^3.

Both polymers in solution show elastic effects and shear-rate dependent viscosity in the semidilute regime ($C>C^*$), although in general, PAA solutions possess larger elastic effects than XG solutions due to the flexible backbone of the former. Hence, by adjusting the solvent viscosity, polymer type, concentration, and imposed strain rate, we are able to investigate the effects of viscoelasticity on mixing with and without the effects of shear-thinning viscosity. Purely viscoelastic effects are investigated by dissolving small amounts of PAA in a viscous solvent to create a constant-viscosity elastic fluid, usually called a Boger fluid[23] and by studying PAA solutions in water below the critical strain rate required to induce shear thinning. The effects of viscoelasticity coupled with shear-thinning viscosity are investigated using high polymer concentration (PAA and XG) aqueous solutions at moderate strain rates. Newtonian fluid mixing is investigated using a glycerol/water solution that matches the viscosity of the Boger fluid.

We use a stress-controlled cone-plate rheometer to characterize the fluids (Fig. 2). A well-known characteristic of viscoelastic fluids is that they exhibit normal stress differences when sheared. The largest of the two normal stress differences is N_1, which in a cone-and-plate geometry causes the cone and the plate to be pushed apart, thus allowing the instrument to measure it directly. At sufficiently low shear rates, N_1 is nearly proportional to the mean square shear rate $\dot{\gamma}^2$ and thus the first normal stress coefficient, given by $\Psi_1 = N_1/\dot{\gamma}^2$, approaches a constant value $\Psi_{1,0}$ at low shear rates [Fig. 2(b)]. For the Boger fluid, a constant Maxwell relaxation time can be defined as $\lambda=\Psi_{1,0}/2\eta$,[31] where η is shear-viscosity. In the case of viscoelastic, shear-thinning fluids, the relaxation time is a function of shear rate, and is defined as $\lambda=N_1/[2\eta(\dot{\gamma})\dot{\gamma}^2]$.

The shear-rate dependent viscosity data [Fig. 2(a)] are fitted to the Carreau viscosity equation, $\eta=\eta_0[1+(\kappa\dot{\gamma})^2]^{-n/2}$, where η_0 is the zero-shear-rate viscosity, n is the power law index and κ is a time constant. The composition and rheological parameters of the various solutions used in the experiments are presented in Table I.

There are four independent dimensionless parameters for this flow. The Reynolds number $\mathrm{Re}=\rho UL/\eta$ is based on the mean magnet spacing $L=2$ cm, rms velocity U, fluid density ρ, and fluid viscosity η. For shear-thinning fluids, we use η measured at the estimated horizontal mean strain rate $\overline{\dot{\gamma}}$ (cf. Fig. 2) in computing the Re. We could alternately use the zero-shear-rate viscosity η_0 instead, but this choice would largely underestimate Re. Since the non-Newtonian fluid viscosity is rate dependent, the use of $\overline{\dot{\gamma}}$ to estimate η seems appropriate. Note that we use the horizontal mean strain rate because the vertical strain rates are negligible in the upper layer.

The path length $p=U/Lf$, where f is the driving fre-

TABLE I. Composition and properties of the solutions used in the experiments. (All solutions also contain 5% KCl by weight.) The measured zero-shear-rate viscosity η_0 is used to calculate the zero-shear-rate relaxation time λ for the shear-thinning fluids. The uncertainties are about 11% for the relaxation times, and about 2% for the exponent n and for κ.

Fluids	Concentration (ppm)	Glycerol (% w/w)	Water (% w/w)	Viscosity (cP)	Relaxation time (λ)	n	κ (s)
Newtonian	···	80	20	90	···	···	···
Boger	100	70	30	90	0.57 s	···	···
Xanthan gum	1000	···	99.9	736	0.31 s	0.69	4.53
PAA I	1500	···	99.85	919	1.4 s	0.72	5.69
PAA II	2500	···	99.75	1268	2.1 s	0.70	7.03

quency of the flow, describes the path length traveled by a fluid element in one forcing period $(1/f)$ normalized by L. The relative importance of elasticity and viscosity is quantified by the Weissenberg number, $\mathrm{Wi}=\lambda\dot{\bar{\gamma}}$, where λ is the fluid relaxation time, which in the case of shear-thinning fluids is a function of shear rate. Note that the *vertical velocity gradient* near the bottom of the cell substantially exceeds the *horizontal gradient* in the upper layer by approximately a factor of 10, so that one might consider defining Wi based on this larger gradient. We do not make this choice because we are studying only the stretching and mixing properties of the thin upper layer, where the vertical velocity gradient has been shown to be small. While for some of our fluids shear thinning will occur near the lower cell boundary, it does not appear to affect the behavior of the upper layer significantly.

Shear-thinning effects in the upper layer are characterized by a dimensionless strain rate $\kappa\dot{\bar{\gamma}}$, where κ, defined previously, is the characteristic time associated with shear-thinning effects. An additional dimensionless parameter, the elasticity number $(\mathrm{El}=\mathrm{Wi}/\mathrm{Re}=\lambda\eta/\rho L^2)$, is sometimes used to characterize the ratio of elasticity to inertial forces.

III. RESULTS

A. Purely elastic fluids

The effects of viscoelasticity (without shear-thinning viscosity) on fluid mixing are investigated using a Boger fluid and a viscosity-matched Newtonian fluid. We begin our analysis by comparing the resulting velocity fields, obtained from particle tracking data, for both cases (Fig. 3) at $\mathrm{Re}\approx 1.2$ and $p=2.1$. Particles typically move distances comparable to the magnet spacing during half a period, though their total displacement in a full period is generally much less. For the geometry and range of Wi considered in this investigation, the velocity field patterns of Newtonian and Boger cases are very similar. This similarity indicates that elasticity has little effect on the flow field, other than slightly reducing the velocity magnitude. More quantitative measures of the similarities among the measured velocity fields are given in Sec. III B.

We calculate stretching fields (Fig. 4) for the Boger and Newtonian solutions from their corresponding velocity fields. The stretching fields are generally large on the stable and unstable manifolds of fixed points, and can be used to predict mixing rates; higher stretching values generally translate into faster mixing rates.[29] We find that the addition of small amounts of elasticity does not modify the structure of the stretching field patterns, i.e., the locations of large stretching. This may be viewed as a consequence of the fact that the velocity patterns are similar. However, the lines of future and past stretching are less intense in the Boger case [Fig. 4(a)]; this fact indicates an overall inhibition of stretching (and consequently mixing), even though Wi is rather small (0.025).

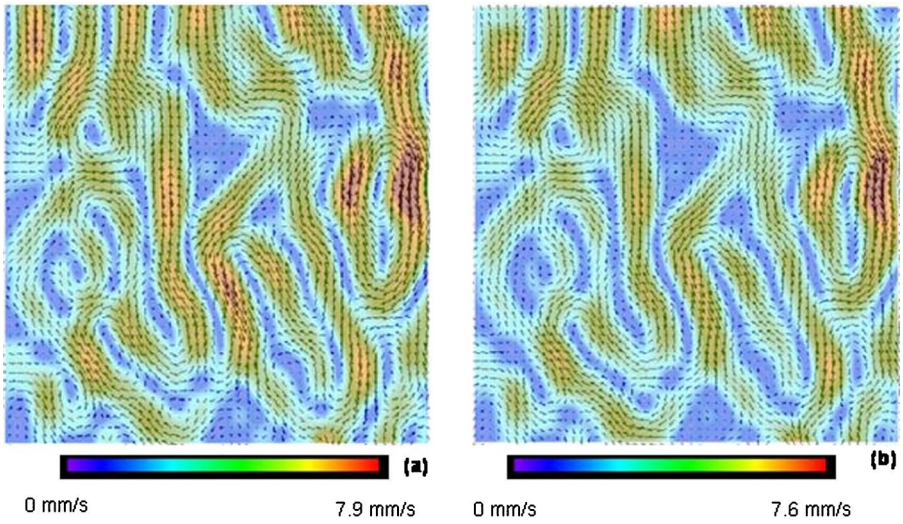

FIG. 3. (Color online). Velocity fields color coded by the magnitude of the velocity (print version: higher velocities correspond to larger arrows) for (a) Newtonian ($\mathrm{Re}=1.24$) and (b) Boger ($\mathrm{Re}=1.17$, $\mathrm{Wi}=0.023$) fluids. Small levels of viscoelasticity do not affect the structure of the velocity field patterns.

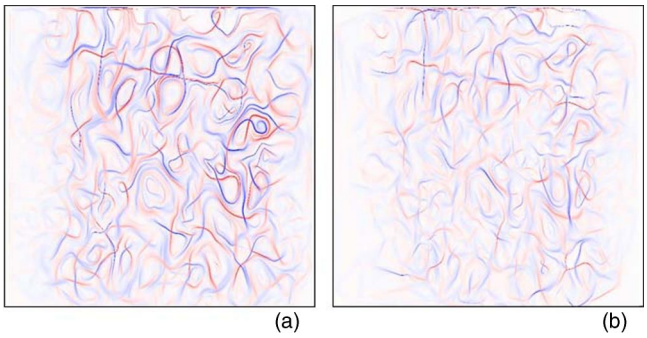

FIG. 4. (Color online). Stretching fields for (a) the Newtonian fluid (Re =1.24) and (b) the Boger solution (Re=1.17, Wi=0.023). The maximum stretching over three periods is shown in color, with future stretching in red, and past stretching in blue (print version: dark lines correspond to regions of high stretching). The mean stretching is larger in the Newtonian case. The starting phase for future stretching, and the ending phase for past stretching, correspond to an instant at which the rms velocity is nearly constant.

In order to quantify the difference in stretching values between the Newtonian and Boger cases, we calculate the mean stretching (sum of all values in the field of view divided by the number of data points) and plot it as a function of Re (Fig. 5). We observe that for the range of Wi studied here, mean stretching is inhibited by elasticity when compared to the viscosity-matched Newtonian case at the same Re (later in this paper we show that the addition of shear thinning changes this picture).

We characterize mixing efficiency by analyzing images containing dye taken once per period. We compute the fractional area covered by the dye on the initially empty half of the cell (5.5×11 cm^2) as a function of time in periods. An example of such plot is given in Fig. 6 for Newtonian and Boger fluids at Re=1.24 and Re=1.17, respectively. The flux of dye into the empty region can be represented by generic curves of the type $A=A_{\max}(1-e^{-KN})$, where A is the area coverage, $A_{\max}$ is the maximum achievable area coverage, K is a dimensionless transport rate (per period), and N is the number of periods. The best fitting transport rates are 0.000 62 for the Newtonian fluid and 0.000 38 for the Boger fluid. The exponential fit for the Boger fluid is shown in Fig. 6, but it is not far from linear over the time interval that we could study. We interpret the slight upward curvature as an artifact related to the fact that we do not image the entire cell. The lower value of K for the Boger case indicates that transport and mixing are suppressed by the addition of polymer, a result that is consistent with the measured reduction in total stretching.

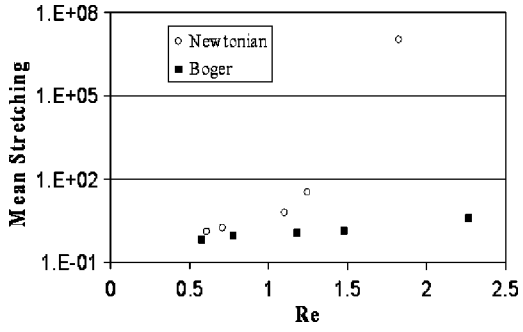

FIG. 5. Mean stretching over the image as a function of Reynolds number for a polymer solution without shear thinning ($0.01<\mathrm{Wi}<0.036$, El=0.02) and a viscosity-matched Newtonian fluid. The mean stretching is reduced for the Boger fluid by elastic stresses (see text).

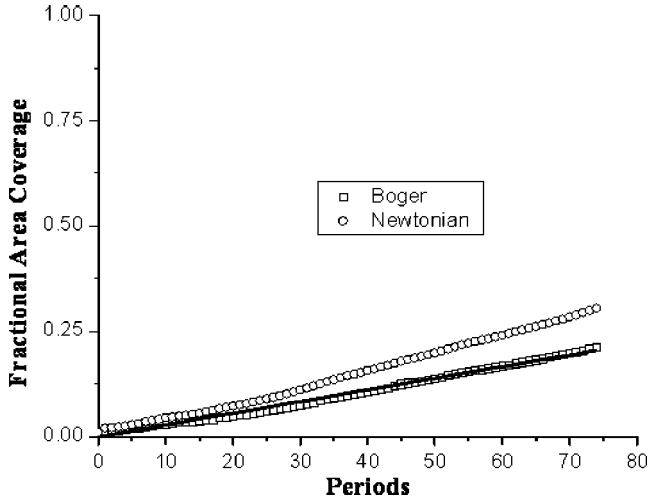

FIG. 6. Fractional area coverage as a function of mixing time (periods) for a polymer solution (without shear thinning) and a viscosity matched Newtonian fluid. The solid line shows an exponential fit. Mixing is somewhat slower for the Boger case.

In summary, our results on the Boger fluid indicate that the addition of small amounts of elasticity to a viscous fluid does not modify the general pattern or form of the velocity and stretching fields, but it inhibits transport, and reduces the mean stretching. In making this comparison, we keep the rms velocity nearly constant.[32] It is interesting to compare these observations to a previous study of chaotic mixing in elastic fluids using a cavity flow.[17] These authors found a lower degree of Lagrangian chaos (i.e., larger regular regions) and slower mixing when compared to a Newtonian fluid. Our observations are consistent with theirs, though the flow is quite different, and the stretching fields were not measured in the earlier work.

B. Shear-thinning fluids

Quite different results are obtained when shear-thinning effects become important. Unlike the constant-viscosity elastic case, the velocity field patterns of shear-thinning fluids are significantly modified when compared to Newtonain fluids at similar Re. The effect of shear-thinning viscosity on the structure of a particular velocity field (say $\vec{V}_1$) can be visualized by plotting the magnitude of the velocity field normalized by the rms velocity (averaged over space),

$$\tilde{V}_1 = \left| \frac{\vec{V}_1}{\sqrt{\langle (V_{1x})^2 + (V_{1y})^2 \rangle}} \right|. \tag{1}$$

The normalized velocity fields are presented in Fig. 7 for Newtonian, Boger, and a shear-thinning, weakly viscoelastic case (xanthan gum solution) at similar Re. Examples are also presented online in movie format so that the time dependence can be seen.[33] It is apparent that the normalized veloc-

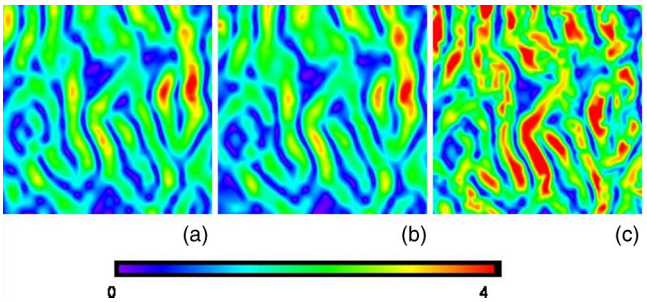

FIG. 7. (Color online). Maps of velocity field magnitudes, normalized by the rms velocity, at different levels of shear thinning when viscoelasticity is small. (a) Newtonian fluid (Re=1.24); (b) Boger fluid (Re=1.47, Wi=0.029); and (c) XG shear-thinning solution (Re=1.1, Wi=0.039, $\kappa\dot{\bar{\gamma}}$=4.9). Note that the Boger and Newtonian solutions have quite similar velocity fields, while the shear-thinning case is quite different, even at comparable Re and small Wi.

ity fields for the Newtonian and Boger fluids presented in Figs. 7(a) and 7(b) are nearly identical. Both of these velocity fields differ substantially from the shear-thinning, viscoelastic case [Fig. 7(c)], where shear-thinning effects are significant. This difference in the velocity field can be largely atributted to shear-thinning rather than elastic effects, since elastic forces are weak (Wi=0.034) and the dimensionless strain rate $\kappa\dot{\bar{\gamma}}$=2.82 is larger than required to produce shear thinning.

We assess the effects of viscoelasticity and shear thinning on the velocity fields by comparing the normalized velocity fields of both Boger and shear-thinning cases to the Newtonian case ($\tilde{V}_2$) by means of difference fields ($|\Delta\tilde{V}| = |\tilde{V}_1 - \tilde{V}_2|$) at matching Re (Fig. 8). We also quantify the differences by calculating the root-mean-square values $\Delta\tilde{V}_{\mathrm{rms}}$, which are shown in Table II. These rms differences show that for the Boger fluid, the velocity field is not affected significantly by the low level of viscoelasticity. On the other hand, weak shearing of the strongly viscoelastic PAA II solution (below the onset of shear thinning) does affect the velocity field, but the effect is much larger at higher strain rate, where shear thinning is also present, while Re remains low.

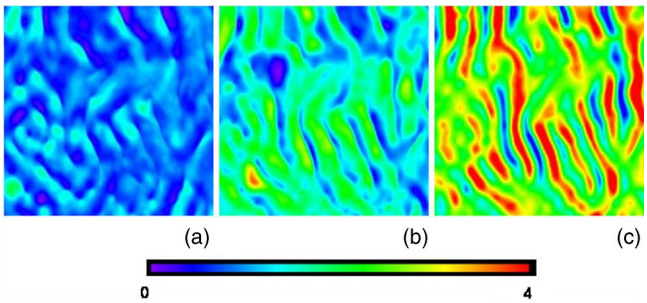

FIG. 8. (Color online). Magnitudes of the velocity field differences (relative to the Newtonian case at the same Re): (a) Boger viscoelastic solution (Re=1.47, Wi=0.029); (b) PAA II solution (Re=0.19, Wi=1.81, $\kappa\dot{\bar{\gamma}}$=0.54); (c) same solution as (b) but at higher strain rate where shear thinning is important (Re=0.4, Wi=3.36, $\kappa\dot{\bar{\gamma}}$=3.2). The velocity fields are modified substantially when both shear-thinning and significant viscoelasticity are present as in (c), but much less by viscoelasticity alone as in (b). See also Table II.

TABLE II. Values of the rms difference in velocity $\Delta\tilde{V}_{\mathrm{rms}}$ (relative to the Newtonian case and averaged over the field of view), for fluids whose viscosities are either constant (the Boger case) or dependent on strain rate. For the Boger fluid, the low elasticity level does not modify the velocity field significantly. Weak shearing of the strongly viscoelastic PAA II solution (below the onset of shear thinning) does affect the velocity field, but the effect is much larger at higher shear rate, where large shear thinning is also present, while Re remains low.

Fluid	Re	El	$\kappa\dot{\bar{\gamma}}$	$\Delta\tilde{V}_{\mathrm{rms}}$
Boger	1.47	0.02	NA	0.057
PAA II	0.19	9.55	0.54	0.17
PAA II	0.4	8.4	3.2	0.61

The substantial changes in the velocity field patterns for the shear-thinning fluids (compared to the Newtonian or Boger case) result in modified stretching field patterns as well, as shown in Fig. 9. We begin by considering the stretching field of a fluid (PAA II) that is elastic (Wi=1.86), but is sheared below the onset of shear-thinning effects ($\kappa\dot{\bar{\gamma}}$ =0.54). In this case, viscoelasticity modifies both the velocity field and the stretching field structure [Fig. 9(b)]. This is expected, since at Wi>1, stretched polymer molecules can act back on the flow. However, we do not observe regions of very large future or past stretching. We consider next the opposite case, for which viscoelastic effects are small (Wi

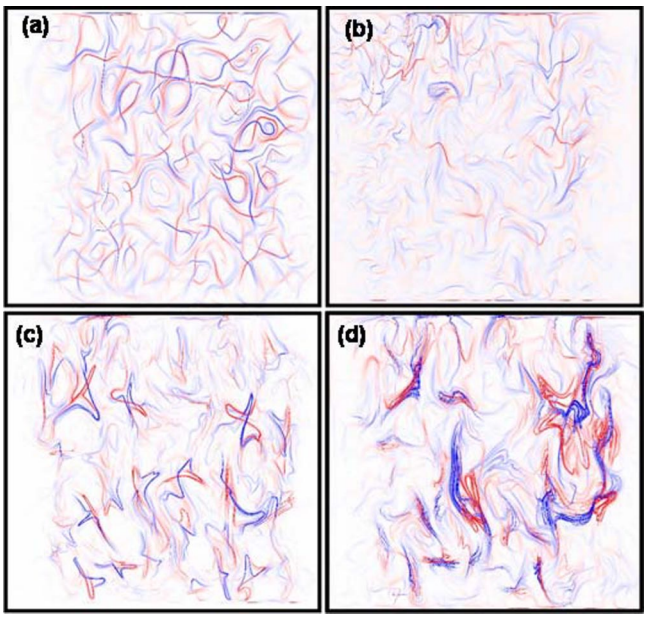

FIG. 9. (Color online). Stretching fields after three periods (print version: dark lines correspond to regions of high stretching). (a) Newtonian fluid (Re=1.24); (b) strongly viscoelastic fluid, PAA II (Re=0.19, Wi=1.86, $\kappa\dot{\bar{\gamma}}$ =0.54); (c) shear-thinning nonviscoelastic fluid, XG (Re=1.68, Wi=0.05, $\kappa\dot{\bar{\gamma}}$=4.8); and (d) both viscoelastic and shear-thinning solution, PAA II (Re=0.385, Wi=2.56, $\kappa\dot{\bar{\gamma}}$=2.9). Both viscoelasticity and shear thinning modify the stretching field structure, but regions of very large stretching are only present when shear-thinning effects are present.

$=0.05$, comparable to the Boger fluid), but the fluid is sheared above the onset of shear thinning ($\kappa\bar{\dot{\gamma}}=4.8$). This case is exemplified by the xanthan gum solution shown in Fig. 9(c). We observe that the stretching field pattern is significantly modified from the Newtonian case, showing a higher concentration of sharp lines of stretching (future and past). Since the Reynolds numbers are close for the Newtonian and xanthan gum fluids [Fig. 9(a), Re$=1.24$; and Fig. 9(c), Re$=1.68$] and viscoelasticity is small, we attribute the changes in the stretching field almost entirely to shear-thinning effects.

Finally, we provide an example of a fluid (PAA II) that is both viscoelastic (Wi$=2.56$ and is sheared above the onset of shear thinning effects ($\kappa\bar{\dot{\gamma}}=2.9$), as shown in Fig. 9(d). In this case, the stretching field structure is strongly modified and we observe the presence of large folds indicating a substantial enhancement of the mean stretching. In general, both viscoelasticity and shear-thinning modify the stretching field structure, but regions of very large stretching are only present when shear-thinning effects are present. These comparisons are made at the same Re.

We observe a substantial enhancement of mean stretching for all of the shear-thinning fluids studied here. The mean stretching values for shear-thinning fluids are shown as a function of Re in Fig. 10(a), where Re is calculated using the viscosity at the actual rms shear rate. Shear-thinning fluids enhance total stretching even at low elasticity levels, as in the rigid xanthan polymer case ($0.015<\mathrm{Wi}<0.06$). More dramatic enhancement in stretching is observed for viscoelastic, flexible PAA cases with Wi varying from 0.6 to 2.6 as Re is varied.

One limitation of these results is that it was not possible to match the path length p in addition to Re when the much more viscous shear thinning fluids are used. Thus, it is important to check to ensure that the increase in mean stretching of shear-thinning fluids is not due solely to the larger distances traveled by a fluid element in one forcing period as the shear rate is increased. This distance is quantified by the path length p. A previous study[29] shows that mixing rate increases with path length at a given Re for a Newtonian fluid in a time-periodic flow. In order to address this issue, we perform experiments in which we match both Re and p of the PAA I fluid to the Boger case by increasing the forcing frequency (decreasing p). We find that shear-thinning effects enhance the mean stretching when compared to purely viscoelastic fluids even when p is held constant, although to a somewhat lesser degree, as is shown by the data points labeled PAA I (p) in Fig. 10(a).

The dependence of the mean stretching on dimensionless strain rate is shown in Fig. 10(b) for all the fluids studied. The pronounced rise at the onset of shear thinning, $\kappa\bar{\dot{\gamma}}>1$ is evident. At higher levels of elasticity (upper two curves), the enhancement of stretching is more pronounced, so both shear-thinning viscosity and elasticity contribute.

Dye mixing experiments confirm that the trends shown by the stretching measurements actually describe mixing. Figure 11 shows images of the evolution of dye mixing for a Newtonian fluid and a shear-thinning, viscoelastic fluid

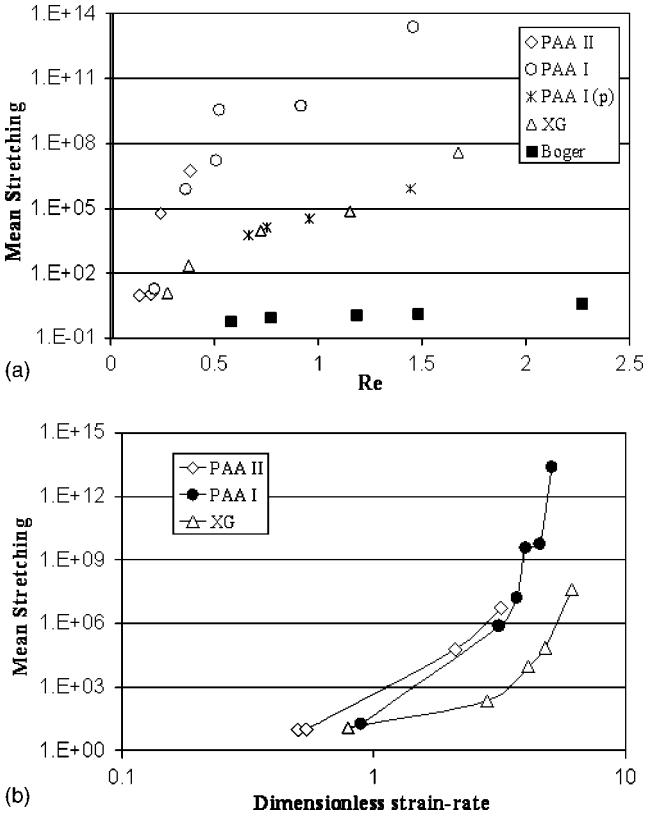

FIG. 10. (a) Comparison of mean stretching (averaged over the image) for shear-thinning fluids with the Boger case. The shear thinning cases (XG, PAA I, and PAA II) show substantial enhancement in stretching. The enhancement remains even when the path length p is matched to the Newtonian and Boger cases; this case is labeled PAA I (p). (b) Mean stretching for shear-thinning fluids as a function of dimensionless strain rate $\kappa\bar{\dot{\gamma}}$. Stretching is substantially enhanced by shear thinning when $\kappa\bar{\dot{\gamma}}>1$.

(PAA I, Wi$=1.09$, $\kappa\bar{\dot{\gamma}}=5.1$) at similar Re. The mixing patterns of both fluids are complex and are markedly different from each other. Careful observation of the images shows that both flows produce mixing structures that, when recorded at periodic intervals, are similar over time, except that the dye contrast decays.[5] There are isolated nonmixing regions in the Newtonian case, but not in the shear-thinning case. The presence of isolated nonmixing regions is an indication of inefficient mixing since they act as barriers to material transport. The overall dye penetration into the initially empty region is much greater for the shear-thinning fluid at comparable times. Curves showing fractional area coverage as a function of time are given in Fig. 12 for Newtonian and shear-thinning viscoelastic fluids at the same Re. The transport rates K for the PAA I solution and Newtonian fluids are 0.043 and 0.000 62, respectively. The transport of dye (per period) into the empty region of the mixing cell is dramatically faster for the shear-thinning viscoelastic fluid than for the Newtonian fluid. This seems reasonable in view of the measured enhancement of total stretching.

C. Local velocity analysis

In order to understand the increase in stretching and mixing for the shear-thinning fluids, and their suppression

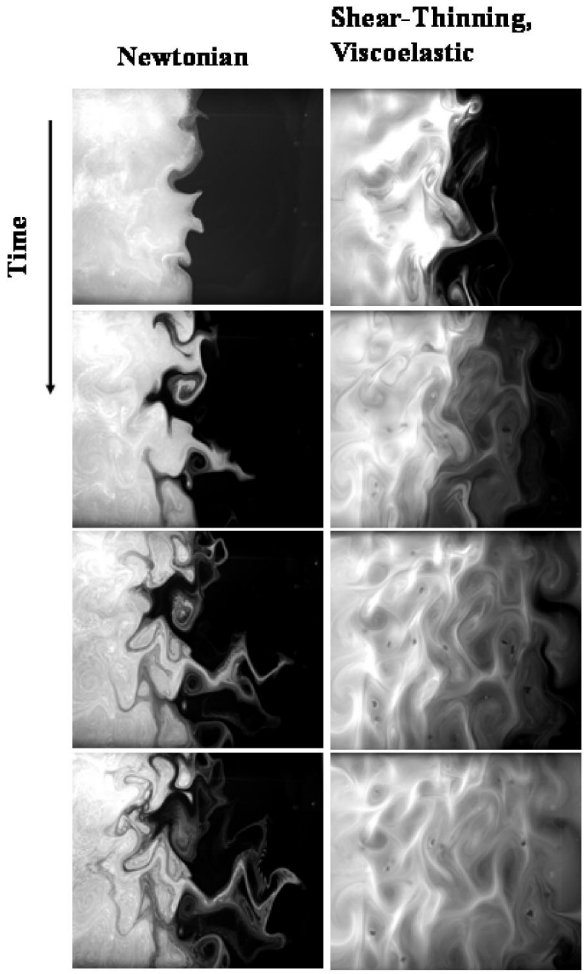

FIG. 11. Images of the dye field showing changes in flow patterns and enhancement of mixing with a shear-thinning fluid. Left column: Newtonian fluid (Re=1.24). Right column: PAA I (Re=1.45, Wi=1.09, $\kappa\dot{\bar{\gamma}}=5.1$). Each row shows an image taken ten periods after the one above it.

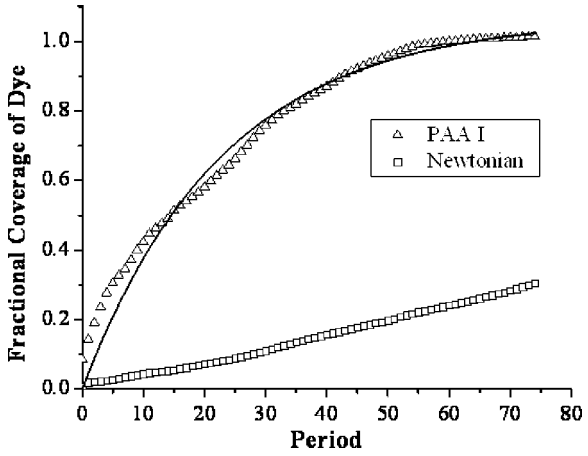

FIG. 12. Fractional area coverage as a function of mixing time (periods) for a shear-thinning polymer solution and a Newtonian counterpart, at the same Re. The solid line shows an exponential fit.

for the Boger fluid, we examine the velocity field with high resolution in both sheared and elongational regions of the flow (Fig. 13). We study a sheared path that extends between two elliptic points, and three elongational paths that pass through hyperbolic points. We compare and study in detail the shear and elongational flow fields of the various polymeric fluids shown in Table I by measuring the velocity along the paths shown in Fig. 13 at similar Re.

We report one normalized velocity component along the selected path s, defined as $\tilde{V}(s)=[V(s)I_N]/(V_N I)$. Here, $V(s)$ is the selected velocity component, V_N is the maximum velocity for a Newtonian reference fluid on the selected path, and I and I_N are the imposed electrical currents used to drive the polymer solution and the Newtonian reference fluid, respectively. The quantity $\tilde{V}(s)$ is the velocity per unit driving current, compared to a Newtonian reference fluid.

We plot the normalized velocity component as a function of distance along the selected path in Fig. 14. In the shear flow region [Fig. 14(a)], using the velocity perpendicular to the selected path, we recover nearly identical parabolic profiles, typical for shear flows, for both Newtonian and Boger fluids at Re$\approx$1.2. This indicates that their shear properties (i.e., shear viscosity) are very similar. On the other hand, for the shear-thinning PAA I solution, the measured normalized shear velocity profile deviates from the Newtonian profile and has a somewhat higher magnitude, particularly at the centerline. The higher magnitude seems to be related to shear thinning, which decreases the flow resistance at locations of high strain rate.

On the other hand, in the hyperbolic or elongational regions of the flow, where we plot the velocity component *parallel* to the selected path, we find lower normalized velocities for the Boger fluid when compared to the Newtonian case at Re$\approx$1.2 [Fig. 14(b)]. This reduced velocity near hyperbolic points for Boger fluids may explain their lower mean stretching and mixing. The implied increase in flow resistance is most likely due to extra elastic stresses, since Re is fairly small.

It is known that the addition of small amounts of high-molecular-weight flexible polymers (PAA) in solution can increase the resistance to flow in extension, even at small

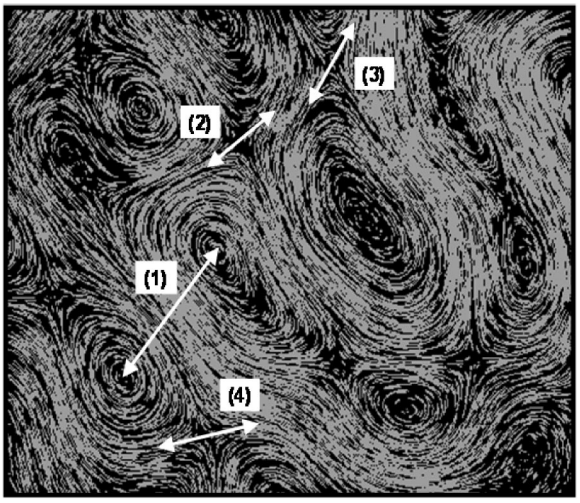

FIG. 13. Flow field of a region of interest within the flow showing a sheared region between two elliptic fixed points (1) and three elongational regions (2–4), passing through hyperbolic fixed points.

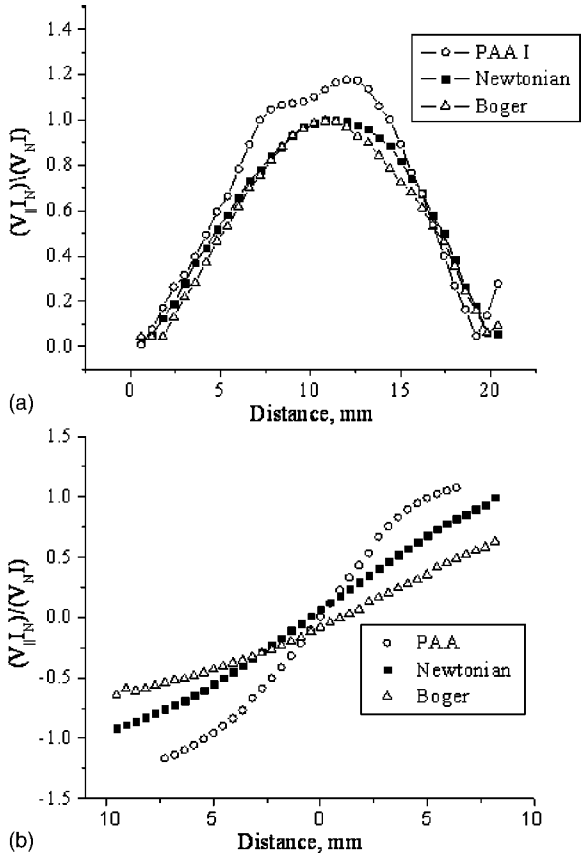

FIG. 14. (a) Normalized *perpendicular* component of the velocity (see text) along the sheared line (1) in Fig. 13. The flow profile is nearly parabolic for both Newtonian and Boger fluids. Small deviations in profile shapes and higher center-line speeds are observed for a shear-thinning fluid (PAA I). (b) Normalized *parallel* velocity profile along the elongational line (4) in Fig. 13. The Boger fluid shows a small speed reduction when compared to the Newtonian fluid; lower speeds in this region may be responsible for a small reduction in mean stretching and reduced mixing. In contrast, the PAA I solution shows a higher elongational velocity, which leads to larger stretching and mixing.

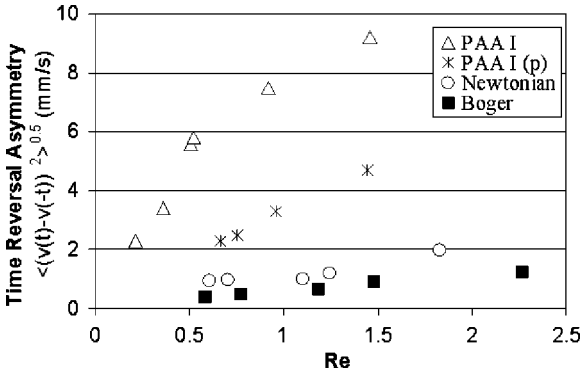

FIG. 15. Measure of the breaking of time reversal symmetry of time-periodic flows, showing that the shear-thinning fluid breaks this symmetry dramatically compared to the Boger and Newtonian cases, at a given Re.

strain rates. The material property that quantifies this resistance to flow in extension is the extensional viscosity η_e. In the case of Newtonian fluids, the extensional viscosity is three times its shear viscosity ($\eta_e=3\eta$), while for high-molecular flexible polymers it can be much larger than three times its shear viscosity ($\eta_e>3\eta$). In this work, although both fluids have nearly identical shear viscosities, the Boger fluid seems to have a slightly larger elongational viscosity than the Newtonian fluid, which is evident in the lower normalized flow velocities near hyperbolic points. By contrast, the semidilute PAA I solution shows higher values of normalized elongational velocity, i.e., shear-thinning elongational behavior. This reduced resistance near hyperbolic points probably contributes to the higher measured stretching of the PAA I solution compared to the Newtonian and Boger fluids at the same Re.

D. Time reversibility

Previous work[29] on Newtonian fluids shows that obtaining large mean stretching (or mixing) requires breaking time reversal symmetry. That is, the velocity of a fluid element must not simply change sign on its return path when the forcing is reversed, so that it does not return to its starting position (even though the velocity field is time periodic).

We measure departures from time reversal symmetry for polymeric solutions by calculating the sum of the local velocities at equal time intervals before and after the zero crossing of the rms velocity. This quantity vanishes if time-reversal symmetry holds. The standard deviation of this quantity, averaged over space and phase, is plotted in Fig. 15. We find that in the Boger case, the breaking of time-reversal symmetry is somewhat reduced. We propose that this reduction is due to the extra elastic stresses (and reduced velocities) near the hyperbolic points In other words, even though the inertial time lags are small at low Re, they are further reduced in the Boger case by elastic stresses.

By contrast, we see in Fig. 15 that shear-thinning viscosity dramatically increases the breaking of time reversibility at a given Re, even if the path length p is also matched. The symmetry breaking grows as either Re or the dimensionless strain-rate increases. Note that the symmetry breaking here is not accompanied by any reduction in time periodicity.

Why does shear-thinning viscosity tend to break time reversal symmetry? There are two possible explanations stemming from two possible sources of time lags. In the Newtonian flow (at finite Re), small inertial lags cause particles not to return to their starting locations, and mixing is observed. For the shear-thinning fluid, even though we make comparisons at the same Re (computed from the viscosity at the mean shear rate) the velocities are larger in some regions of the flow than for the Newtonian fluid (and lower in other regions). Therefore it is possible that the inertial lags are enhanced, though they should be small at low Re, as in the Newtonian case. However, another source of time lags may also be acting at low Re when $\kappa\bar{\dot{\gamma}}>1$. As a fluid element travels between regions with different strain rates, its effective viscosity evolves on a time scale λ for fluids possessing memory. (In the limit of vanishing viscoelasticity, the changes in viscosity associated with shear thinning would be instantaneous.) Therefore, the effective viscosity of a transported fluid element may lag behind the value that would

normally be associated with the local strain rate. These lags could lead to a breaking of time-reversal symmetry, and this effect could be the larger one at low Re.

IV. SUMMARY AND CONCLUSIONS

In this paper, we present an experimental investigation of mixing of viscoelastic fluids, with and without shear thinning, in time-periodic flows. Mixing is characterized by means of stretching fields computed from gradients of velocity fields, and also by dye mixing experiments. We find that viscoelasticity alone (the Boger case) modifies the velocity fields only slightly, when compared to a Newtonian case with similar viscosity. Mean stretching and dye transport are mildly suppressed by elasticity (Fig. 5). We document an increase in flow resistance near hyperbolic points for Boger fluids that may account for their lower mean stretching and mixing (Figs. 13 and 14).

On the other hand, we show that when shear thinning is also present, as for the PAA and XG solutions, the flow field is dramatically changed (as shown in Figs. 7 and 8), and both stretching (Fig. 10) and mixing (Figs. 11 and 12) are enhanced. We trace the enhancement of stretching for shear-thinning solutions to a reduced flow resistance (or increased velocity) near hyperbolic points (Figs. 13 and 14) at a given Re. We find that the enhancement of stretching is accompanied by larger breaking of time reversibility even at low Re (Fig. 15). Finally, we argue that the augmented temporal symmetry breaking is caused by time lags produced by either of two mechanisms (or both): (a) the finite elastic relaxation time of a fluid element in conjunction with its varying effective viscosity as it is transported or (b) inertial effects.

These experimental results show that enhanced mixing (compared to the Newtonian) (case at the same Re) can occur for low elasticity, as long as shear-thinning effects are present, as is the xanthan gum case. This fact is of importance when dealing with semidilute solutions containing cells, polymers (flexible or not), or particles, where strain-rate dependent viscosity is common. Shear-thinning effects can also potentially be important when dealing with semidilute non-Newtonian fluids in microdevices, due to the large shear rates often encountered in these situations.

ACKNOWLEDGMENTS

The authors appreciate helpful discussions with Morton Denn, Daniel Joseph, and Gary Leal. Benjamin Bigger and Timothy Saint contributed to these experiments at an early stage. Michael Rivera suggested important instrumental improvements. This work was supported by the NSF Division of Materials Research under Grants No. DMR-0072203 and No. DMR-0405187.

[1] H. Aref, "Stirring by chaotic advection," J. Fluid Mech. **143**, 1 (1984).
[2] J. M. Ottino, *The Kinematics of Mixing: Stretching, Chaos, and Transport* (Cambridge University Press, Cambridge, 1989).
[3] F. J. Muzzio and P. D. Swanson, "The statistics of stretching and stirring in chaotic flows," Phys. Fluids A **3**, 822 (1991).
[4] W. L. Chien, H. Rising, and J. M. Ottino, "Laminar mixing and chaotic mixing in several cavity flows," J. Fluid Mech. **170**, 355 (1986).
[5] D. Rothstein, E. Henry, and J. P. Gollub, "Persistent patterns in transient chaotic fluid mixing," Nature (London) **401**, 770 (1999).
[6] J. Chaiken, R. Chevray, M. Tabor, and Q. M. Tan, "Experimental study of Lagrangian turbulence in Stokes flow," Proc. R. Soc. London, Ser. A **408**, 165 (1986).
[7] I. C. Walton and S. H. Bittleston, "A comparative computational and experimental study of chaotic mixing in viscous fluids," J. Fluid Mech. **222**, 39 (1991).
[8] R. G Larson, E. S. G. Shaqfeh, and S. J. Muller, "Purely elastic instability in Taylor–Couette flow," J. Fluid Mech. **218**, 573 (1990).
[9] Y. L. Joo and E. S. G. Shaqfeh, "Viscoelastic Poiseuille flow through a curved channel: A new elastic instability," Phys. Fluids A **3**, 1691 (1991).
[10] J. A. Byars, A. Oztekin, R. A. Brown, and G. H. McKinley, "Spiral instabilities in the flow of highly elastic fluids between rotating parallel disks," J. Fluid Mech. **271**, 174 (1994).
[11] E. S. G. Shaqfeh, "Purely elastic instabilities in viscometric flows," Annu. Rev. Fluid Mech. **28**, 129 (1996).
[12] A. Groisman and V. Steinberg, "Mechanisms of elastic instabilities in Couette flow of polymer solutions: Experiments," Phys. Fluids **10**, 2451 (1998).
[13] J. R. Stokes, L. J. W. Graham, N. J. Lawson, and D. V. Boger, "Swirling flow of viscoelastic fluids. Part 2. Elastic effects," J. Fluid Mech. **429**, 117 (2001).
[14] R. G Larson, S. J. Muller, and E. S. G. Shaqfeh, "The effect of fluid rheology on the elastic Taylor–Couette instability," J. Non-Newtonian Fluid Mech. **51**, 195 (1994).
[15] A. Lindner, D. Bonn, and J. Meunier, "Viscous fingering in a shear-thinning fluid," Phys. Fluids **12**, 256 (2000).
[16] J. Wang and D. D. Joseph, "Lift forces on a cylindrical particle in a plane Poiseuille flow of shear thinning fluids," Phys. Fluids **15**, 2267 (2003).
[17] C. W. Leong and J. M. Ottino, "Increase in regularity by polymer addition during chaotic mixing in two-dimensional flows," Phys. Rev. Lett. **64**, 874 (1990).
[18] T. C. Niederkorn and J. M. Ottino, "Mixing of a viscoelastic fluid in a time-periodic flow," J. Fluid Mech. **256**, 243 (1993).
[19] F. H. Ling and X. Zhang, "Mixing of a generalized Newtonian fluid in a cavity," J. Fluids Eng. **117**, 75 (1995).
[20] S. Kumar and G. M. Homsy, "Chaotic advection in creeping flow of viscoelastic fluids between slowly modulated eccentric cylinders," Phys. Fluids **8**, 1774 (1996).
[21] Y. Fan, R. I. Tanner, and N. Phan-Thien, "A numerical study of viscoelastic effects in chaotic mixing between eccentric cylinders," J. Fluid Mech. **412**, 197 (2000).
[22] T. C. Niederkorn and J. M. Ottino, "Chaotic mixing of shear-thinning fluids," AIChE J. **40**, 1782 (1994).
[23] D. V. Boger, "Highly elastic constant-viscosity fluid," J. Non-Newtonian Fluid Mech. **3**, 87 (1977).
[24] A. Groisman and V. Steinberg, "Efficient mixing at low Reynolds numbers using polymer additives," Nature (London) **410**, 905 (2001).
[25] A. B. Metzner and R. E. Otto, "Agitation of non-Newtonian fluids," AIChE J. **3**, 3 (1957).
[26] A. W. Nienow and T. P. Elson, "Aspects of mixing in rheologically complex fluids," Chem. Eng. Res. Des. **66**, 5 (1988).
[27] J. R. Stokes and D. V. Boger, "Mixing of viscous polymer liquids," Phys. Fluids **12**, 1411 (2000).
[28] G. A. Voth, G. Haller, and J. P. Gollub, "Experimental measurements of stretching fields in fluid mixing," Phys. Rev. Lett. **88**, 254501 (2002).
[29] G. A. Voth, T. C. Saint, G. Dobler, and J. P. Gollub, "Mixing rates and symmetry breaking in two-dimensional chaotic flow," Phys. Fluids **15**, 2560 (2003).
[30] J. Paret, D. Marteau, O. Paireau, and P. Tabeling, "Are flows electromagnetically forced in thin stratified layers two dimensional?" Phys. Fluids **9**, 3102 (1997).
[31] R. B. Bird, C. F. Curtiss, R. C. Armstrong, and O. Hassager, *Dynamics of Polymeric Liquids: Fluid Mechanics*, Vol. 1, 2nd ed. (Wiley, New York, 1987).
[32] It is difficult to reproduce the rms velocity perfectly due to conductivity variations; it varies by up to 6% from run to run. However, these variations are not enough to affect our conclusions.
[33] See EPAPS Document No. E-PHFLE6-17-045505 for video animations of the velocity fields. This document can be reached via a direct link in the online article's HTML reference section or via the EPAPS homepage (http://www.aip.org/pubservs/epaps.html). Video animations of the velocity fields are also available at www.haverford.edu/physics-astro/gollub/polymer_mixing.